A&A, 708, A369 (2026)
https://doi.org/10.1051/0004-6361/202557884

Astronomy & Astrophysics

Measuring Titan's rapid orbital expansion combining Cassini radio science normal points and astrometry

Andrea Magnanini[1,⋆], Valery Lainey[2], Luis Gomez Casajus[1,3], Marco Zannoni[1,3], and Paolo Tortora[1,3]

[1] Dipartimento di Ingegneria Industriale, Alma Mater Studiorum - Università di Bologna, 47121 - Forlì (FC), Italy
[2] LTE, Observatoire de Paris, PSL Research University, CNRS, Sorbonne Université, Université de Lille 1, Paris, France
[3] Centro Interdipartimentale di Ricerca Industriale Aerospaziale, Alma Mater Studiorum - Università di Bologna, 47121 - Forlì (FC), Italy

Received 28 October 2025 / Accepted 23 February 2026

ABSTRACT

Recent analyses of Titan's orbital migration have yielded conflicting results regarding Saturn's tidal dissipation (Q) at Titan's frequency. While some studies reported a low Q consistent with resonance locking using independent radio science and astrometric datasets, subsequent work combining multiple mission datasets found a significantly higher Q, disagreeing notably with the earlier radio science findings. This study re-evaluates Titan's migration by integrating Cassini radio science data, processed as normal points, with over a century of astrometric observations within a unified dynamical model using NOE software. Our combined analysis confirms the previously reported rapid migration rate and low Q, thus supporting the nonclassical dissipation mechanisms hypothesis.

Key words. astrometry – celestial mechanics – ephemerides – planets and satellites: dynamical evolution and stability

1. Introduction

The migration of Saturn's largest moon Titan has drawn considerable attention as its measured expansion rate from Lainey et al. (2020) appears to exceed the predictions based on classical tidal theories (Goldreich & Nicholson 1977; Dermott 1979). They proposed that resonance locking, where Titan interacts with Saturn's internal inertial waves, provides a plausible mechanism for this rapid migration (Fuller et al. 2016). Their findings suggested a much smaller tidal quality factor Q for Saturn at Titan's frequency than traditionally expected. The analysis is based on two independent methods and datasets: (1) radio science data acquired during the gravity Titan flybys of Cassini, analyzed using the MONTE software (method 1); (2) classical astrometry data, collected over more than a century, analyzed with the NOE software (method 2). While both methods produced statistically coherent results, the radio science solution yielded results that were significantly more precise than the astrometry solution, finding $Q = 124^{+26}_{-19}$ (3σ). Jacobson (2022), in a comprehensive analysis of the Saturnian satellite system merging the datasets of astrometry and radio science of Cassini, Voyager, and Pioneer 11, obtained a result that diverged by one order of magnitude from the results of Lainey et al. (2020), obtaining $Q = 1224 \pm 357$ (3σ). Instead, considering the astrometry dataset only, hence removing the radio science data of Cassini and Voyager, the estimated central value of Q became compatible with method 2 of Lainey et al. (2020). However it remained statistically compatible with zero, finding Q=91±303 (3σ). Jacobson (2022) found that to determine Saturn's dissipation at Titan's frequency, radio science data were essential, but only by combining Voyager 1 data with Cassini's, given that Cassini data alone proved insufficient in that analysis. This made the radio science data result an important discrepancy to resolve with respect to Lainey et al. (2020).

Jacobson (2022) raised valid concerns mainly about two aspects of radio science analyses in Lainey et al. (2020): (1) the indirect measurements of Saturn gravity field, which could not be estimated directly from only the radio science data of Titan's flybys; (2) the reliance on limited time span datasets, which may be too short to separate the tidal acceleration from long-term periodic gravitational perturbations. To address this discrepancy, we conducted a third investigation that overcomes these two limitations by combining Cassini's radiometric tracking data with long-term astrometric observations, thus ensuring that all observations are analyzed within a consistent dynamical framework. The radio science data are inserted into the astrometric dataset in NOE, as normal points generated by a local approach (see Section 2.1), the same approach used in Folkner et al. (2014) and Park et al. (2021) for planetary ephemerides when using data from spacecraft flybys. By generating these points using a local, per flyby approach, we effectively decouple them from a global dynamical model during the pre-processing stage. The associated a priori uncertainties are deliberately conservative to account for this independence. In the subsequent step, these normal points are ingested into the NOE software alongside the astrometric dataset. At this stage, all observations (both the radio science normal points and the classical astrometry) are analyzed against a single, consistent dynamical model of the Saturnian system to derive the final dissipation parameters. Our approach is a practical and conservative alternative to a full global inversion, while a global inversion might yield smaller uncertainties. This new study mitigates potential biases arising from limited data coverage, and directly solves for the main gravitational parameters of Saturn that were not directly estimated in the radio science analysis of Lainey et al. (2020) (for more details, see Sect. 2.3).

⋆ Corresponding author: andrea.magnanini3@unibo.it

2. Methods

2.1. Radio science normal point generation

The normal points method consists of an estimation of the state of Titan, both position and velocity, with respect to Saturn at the closest approach of each gravity-dedicated Cassini flyby of Titan, and exploiting radio tracking data (Doppler and range) when available in the vicinity of the closest approaches (the Cassini radio tracking data are publicly available through NASA's Planetary Data System[1]). The estimation of these normal points was performed by means of an orbit determination analysis, exploiting the multi-arc approach, as done in the past by the Cassini Radio Science team for gravity field experiments (Iess et al. 2012; Tortora et al. 2016; Durante et al. 2019; Zannoni et al. 2020; Lainey et al. 2020; Petricca et al. 2025). To measure a precise state Titan at each arc and estimate its gravity field, we analyzed the Cassini radiometric data acquired during ten dedicated gravity flybys (T11, T22, T33, T45, T68, T74, T89, T99, T110, and T122) throughout the mission. The primary observable used in the trajectory reconstruction is the spacecraft range rate, extracted from the Doppler shift of a microwave carrier transmitted from Earth at *X*-band (7.2 GHz) and coherently retransmitted by the spacecraft at both *X*-band (8.4 GHz) and *Ka*-band (32.5 GHz). The Doppler observables were compressed at a count time of 60 s. In our data selection strategy, we prioritized two-way Doppler data over three-way data due to their higher intrinsic stability. Three-way data were included only when two-way links were unavailable, estimating an inter-station clock offset bias in the filter. Similarly, *X/Ka* band measurements were preferred over *X/X* band when available, as the higher downlink frequency is less sensitive to dispersive noise caused by the solar plasma and Earth's ionosphere. Range data were also considered at 60 seconds, mostly important in order to constrain Titan's state. We corrected for Earth's tropospheric and ionospheric delays using Global Positioning System data and Advanced Water Vapor Radiometer calibrations, when available (Bar-Sever et al. 2007). When these were unavailable, the Tracking System Analytical Calibration (TSAC) was employed. To prevent biases from inaccurate media calibrations, we discarded tracking data acquired at elevation angles lower than 15°. Additionally, corrections were generated to account for the Doppler shift induced by the spin of the Cassini spacecraft. The data were weighted based on the root mean square of the observation residuals for each tracking pass. The analysis focused on data arcs spanning approximately two to five days around the closest approach, excluding periods containing orbit correction maneuvers or reaction wheel desaturation events. The orbit determination was performed using the Jet Propulsion Laboratory's MONTE software (Evans et al. 2018), applying a linearized weighted least-squares filter to refine the spacecraft's dynamical parameters. The residuals of all the radio tracking data considered are shown in Figs. A.1 and A.2.

We modeled the spacecraft dynamics within a relativistic framework, including the primary gravitational accelerations from the Sun, the Solar System planets, and Saturn's major moons. For both Saturn and Titan, the gravity fields accounted for the spherical harmonic expansions of their gravity fields. Specifically, Titan's gravity field was expanded to degree and order 5, incorporating degree-2 time-varying tidal effects parameterized by the tidal Love number k_2.

Titan's rotational state was imposed considering the classical synchronous rotation model described in Lainey et al. (2019) and Magnanini et al. (2024). Saturn's gravity field and rotational state were assumed to be consistent with the latest SAT441 ephemerides model[2]. For nongravitational forces, we included the solar radiation pressure, atmospheric drag using the recently revised Titan Global Reference Atmosphere Model (Titan-GRAM) (Petricca et al. 2025), and the thermal recoil acceleration induced by the radioisotope thermoelectric generators (RTGs), adopting the standard model from previous Cassini analyses (Durante et al. 2019; Goossens et al. 2024; Petricca et al. 2025).

In the multi-arc approach, data acquired during different flybys are jointly analyzed to estimate a set of global parameters that are constant for all the encounters, and local parameters that influence the single flybys. The global parameters included Titan's gravity field up to order and degree 5, Saturn's GM and J_2, and Cassini's RTGs acceleration, where the a priori uncertainties are set large, so as not to constrain the solution. The local parameters included the state of both Titan and Cassini at the beginning of each flyby. Relatively large a priori uncertainties were used for Titan, 5 km in position and 50 cm/s in velocity, while for the Cassini spacecraft, the uncertainties were 20 km in position and 0.2 m/s in velocity. The initial state of Titan is from the satellitary ephemerides SAT441; Saturn's position is from the planetary ephemerides DE440 (Park et al. 2021)[3]. Regarding nongravitational forces, we estimated scale factors for solar radiation pressure and the atmospheric drag coefficient of the spacecraft, assigning a priori uncertainties of 10% to both. Additionally, the T110 flyby required a specific calibration due to the use of the LGA for tracking. To account for the Doppler signal generated by the antenna's rotation around the center of mass, we included the LGA phase center coordinates as estimated parameters, as done in previous analyses (Durante et al. 2019; Petricca et al. 2025).

Importantly, treating Titan's state as a local parameter allows observations that closely approximate its raw position at each closest approach without relying heavily on a specific dynamical model. This local approach is largely insensitive to dissipative parameters and the detailed dynamical model of the moons, as the integration period is not long enough for these effects to manifest significantly in the data. By estimating Titan's state independently for each flyby, the retrieved uncertainty for Titan's position is notably higher compared to a global approach (Magnanini 2021), where Titan's ephemeris is coherently determined across all flybys. While this method yields more conservative results, it is straightforward to implement within the NOE software and was deemed an effective compromise for the scope of this analysis. The estimated gravity field coefficients and Love number k_2 are completely compatible with Durante et al. (2019) and Petricca et al. (2025); the full solution is reported in Table C.2. The reduced normal points are summarized in Table C.1, together with their correlation matrix in Fig. C.1. Figure 1 compares the normal points against the reference ephemerides SAT441 (Jacobson 2022) in the radial, tangential, and normal directions, showing differences not exceeding 1σ for all the points, with the exception of T074, which is almost 2σ.

2.2. Astrometric dataset update

Building on prior work (Lainey et al. 2020), we analyzed a comprehensive dataset spanning over a century, from 1886 through

[1] https://atmos.nmsu.edu/pdsd/archive/data/

[2] https://ssd.jpl.nasa.gov/ftp/misc/pck/pck.sat441.tpc

[3] ftp://ssd.jpl.nasa.gov/pub/eph/

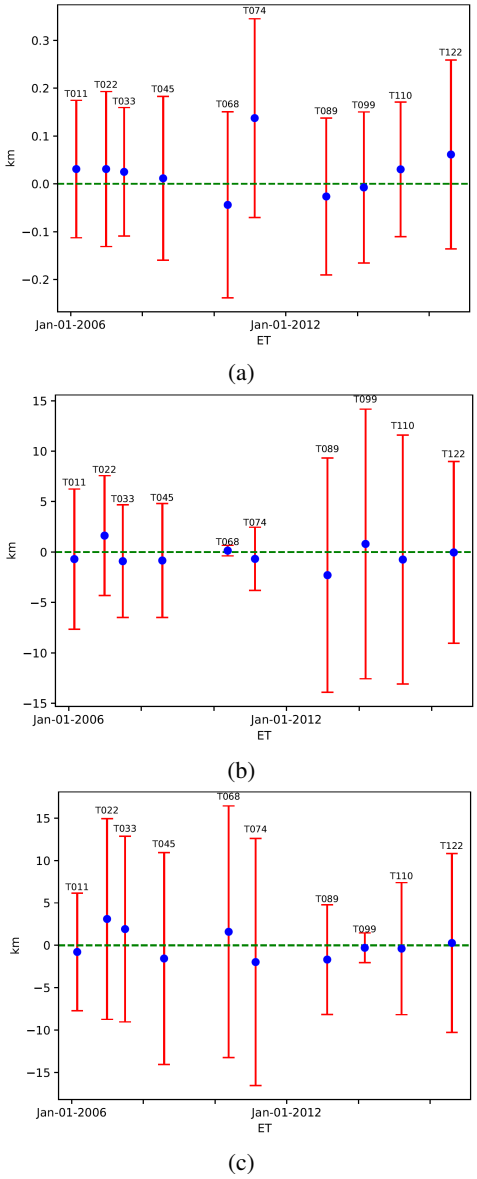

Fig. 1. Comparison of the local normal points for Titan's state relative to Saturn barycenter against the JPL SAT441 ephemeris (Jacobson 2022). The residuals are decomposed into (a) radial, (b) tangential, and (c) normal components. The blue circles denote the deviation of the local solution from the ephemeris, while the red error bars indicate the 3σ uncertainty.

the entirety of the Cassini mission. The presented solution integrates historical ground-based records with high-precision space measurements. A substantial portion of the data is derived from the Cassini mission, specifically incorporating a large set of Imaging Science Subsystem (ISS) observations (Tajeddine et al. 2013, 2015; Cooper et al. 2014, 2018; Zhang et al. 2018). These modern data are complemented by imaging from the Voyager 1 and 2 flybys, and Hubble Space Telescope (French et al. 2006) astrometry. Regarding historical ground-based observations, the study utilizes the comprehensive catalog defined in Desmars et al. (2009), significantly augmented by a new reduction of United States Naval Observatory (USNO) photographic plates covering the period 1974–1998 (Robert et al. 2016) and extra data of the Lagrangian moons (Oberti et al. 1989; Veiga & Vieira Martins 2000; Veiga et al. 2003). We also incorporated recent observations of Hyperion from *Gaia* data (Tanga et al. 2023). This addition is significant due to the orbital resonance between Hyperion and Titan (Ćuk et al. 2013), which provided a slight improvement in the error bars of Titan's orbital state.

2.3. Dynamical model and filter setup

The dynamical model for the Saturnian satellites used in this work follows Lainey et al. (2020), incorporating relativistic point-mass gravitational accelerations from the Sun, the planets, the Moon, and the major Saturnian satellites. Additionally, it included the gravity field of Saturn and its planetary rings, as determined from the analysis of data collected during the Cassini mission's Grand Finale orbits, and the degree-2 gravity harmonics of Saturn's satellites. Saturn's tidal response to the gravitational influence of Mimas, Enceladus, Tethys, Dione, Rhea, and Titan was modeled using the time-lag approach Mignard (1979). This comprehensive model was used to solve for the equations of motion for Saturn's eight major moons, while also including the four Lagrangian moons of Dione and Tethys, as well as Methone and Pallene. The Lagrangian moons contributed to refining Saturn's Love number (k_2), while Methone and Pallene offered high sensitivity to both Mimas's mass and Saturn's gravity field. Additionally, perturbations from the innermost moons – Prometheus, Pandora, Janus, and Epimetheus – were incorporated through their respective ephemerides (Lainey et al. 2023). We solved for the key gravitational and dynamical parameters that govern the system: the masses of Saturn's moons, Saturn's GM within the uncertainties of Jacobson (2022), Saturn's gravity field zonal harmonics up to order 10 within the uncertainties from Iess et al. (2019), and the orientation and precession rate of Saturn's pole constrained by the uncertainties provided in French et al. (2017). Moreover, the tidal interactions between Saturn and its moons were parameterized by solving for Saturn's tidal Love number k_2 (assuming $k_{2,0} = k_{2,1} = k_{2,2}$) and the tidal dissipation factor $\frac{k_2}{Q}$, specifically at the tidal frequencies corresponding to Mimas, Enceladus, Tethys, Dione, Rhea, and Titan. By doing so, it provides a self-consistent estimate of all the main dynamical and gravity parameters that influence Titan dynamics, which were a limit only in the Lainey et al. (2020) analysis of Cassini tracking data. Importantly, performing independent, unconstrained fits for the aforementioned gravity and pole parameters does not provide any real change in our estimates for Saturn's tidal dissipation and k_2.

3. Results

Our main findings on the Saturn tidal response and dissipation at Titan's frequency are shown in Fig. 2 and Table 1. The fitted body masses are reported in Table B.1, while the solution residuals are shown in Figures B.1 and B.2. With this combined analysis we measured the tidal quality factor of Saturn which drives Titan migration to be $Q = 75^{+176}_{-31}$ (3σ uncertainties), and Saturn's Love number $k_2 = 0.382 \pm 0.017$. The derived quality factor Q, being at the denominator in the tidal force equations, has a nonlinear error, where the absolute uncertainty scales approximately with Q^2, resulting in an increasingly larger uncertainty with larger Q values. The impact of including the Cassini normal points is therefore most clearly quantified by the uncertainty on the dissipation factor, $\frac{k_2}{Q}$. In Table 1 a reduction in its error bar of approximately 25% is shown with respect the astrometry-only solution; the update in the astrometry setup described in Section 2.2 brings a contribution to Saturn's

Table 1. Summary of the results on Saturn's k_2 and Q at the frequency of Titan from this work and from previous analyses.

Parameter	Lainey et al. (2020) *Radio science*	Lainey et al. (2020) *Astrometry*	Jacobson (2022) *Astrometry*	Jacobson (2022) *Radio + Astrometry*	**This work** ***Normal points + Astrometry***
k_2	0.382 ± 0.017	0.382 ± 0.017	0.3830 ± 0.0252	0.3830 ± 0.0252	$\mathbf{0.382 \pm 0.017}$
Q	124^{+26}_{-19}	61^{+240}_{-31}	91 ± 303	1224 ± 357	$\mathbf{75^{+176}_{-31}}$
k_2/Q ($\times 10^4$)	30.8 ± 5.5	69 ± 57	42.0 ± 139.5	3.13 ± 0.939	$\mathbf{50.3 \pm 35}$

Notes. All the displayed uncertainties are 3σ. The a priori σ for the parameters are kept large so as not to constrain the solution.

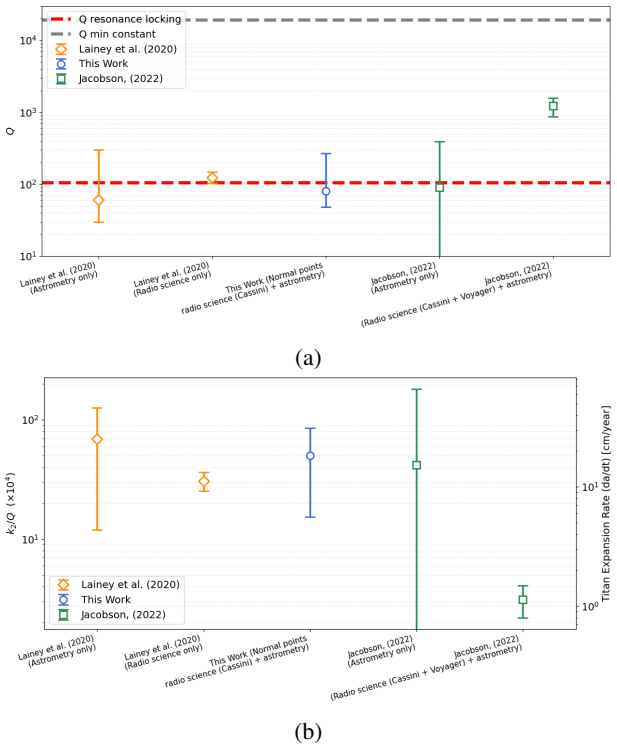

Fig. 2. Tidal parameters of Saturn. (a) Comparison of Saturn's tidal factor ($\frac{k_2}{Q}$) at Titan's orbital frequency from different studies. The results from this work (blue) are compared with those from Lainey et al. (2020) (yellow) and Jacobson (2022) (green). The right vertical axis shows the corresponding rate of orbital expansion for each $\frac{k_2}{Q}$ value. (b) Effective tidal quality factor (Q) of Saturn. The red dotted line indicates the predicted Q from a resonance-locking model, assuming a Saturn evolution timescale of tp=6 Gyr (Lainey et al. 2020). The gray dashed line represents the minimum constant Q value required for the coeval formation of Mimas and Saturn (Lainey et al. 2020).

dissipation error bar with respect Lainey et al. (2020) of approximately 15%. The results confirm the findings of Lainey et al. (2020) regarding Titan's fast orbital migration, which remains incompatible with classical tidal theory. Our solution is fully consistent with their method 1 (radio science-only solution) within 1.1σ in terms of Q.

Notably, our setup is not fully sensitive to Titan's internal dissipation; therefore, we assumed it to be zero, ensuring consistency with Lainey et al. (2020) and Jacobson (2022). Because Titan's internal dissipation would induce a contraction of its semimajor axis, the dissipation value we determine for Saturn serves strictly as a lower bound. For instance, considering the recent estimate of Titan's dissipation by Petricca et al. (2025), Saturn's dissipation would need to be correspondingly stronger to produce Titan's observed orbital expansion. This would result in a Saturnian Q of approximately 55 at Titan's frequency, further reinforcing the hypothesis of strong dissipation within Saturn.

Furthermore, Titan is in synchronous rotation with its orbit. We adopted the classical synchronous rotation model employed by Lainey et al. (2019) (Eq. (22)), where the prime meridian points approximately toward the empty focus of the orbit. Under this assumption, to remain consistent with a null tidal dissipation in Titan, it is fundamental to set the gravity harmonic $S_{2,2} = 0$. Within this rotational model, $S_{2,2}$ is the only static degree-2 gravity parameter that induces a secular effect on the satellite's orbit, specifically on the semimajor axis, as demonstrated by Eq. (43) in Magnanini et al. (2026). As explained by Magnanini et al. (2026), this term should only appear in the presence of tidal dissipation due to the coupling between orbit and rotation. A nonzero $S_{2,2}$ represents a small constant offset between the body-fixed frame and the principal axis frame around the spin axis. This corresponds to a rigid body rotation; in the absence of tidal dissipation, it would cause secular changes in the system's orbital energy and angular momentum without any driving physical phenomena (e.g., stress and strain induced by a varying tidal potential) (Magnanini et al. 2026).

Our analysis allows us to infer Saturn's tidal dissipation from its impact on Titan's orbit, specifically through the secular drift in longitude, which evolves quadratically as the semimajor axis increases linearly due to Saturnian tides. Consequently, neglecting the coupling with the $S_{2,2}$ coefficient can introduce a significant bias in the inferred dissipation. Part of the tidal signal, or even its entirety, could be erroneously absorbed by the $S_{2,2}$ term. An in-depth explanation of this effect and the derivation of the associated formulas can be found in Magnanini et al. (2026).

4. Conclusions

In this study, we successfully merged Cassini radio science normal points with over a century of astrometric observations using the NOE software, creating a unified and consistent dynamical framework. This approach overcomes the limitations of earlier analyses (Lainey et al. 2020) by addressing concerns about the time span of radio science data and the indirect estimation of Saturn's gravitational parameters, as raised by Jacobson (2022). By incorporating both datasets, we solved for all the primary dynamical and gravitational parameters of Saturn and its major moons, providing a more comprehensive understanding of the system. Our results confirm the findings of Lainey et al. (2020), with a tidal quality factor $Q = 75^{+176}_{-31}$

(3σ uncertainty) and k_2=0.382±0.017 supporting the hypothesis of resonance locking as the driver of Titan's rapid migration. These findings are incompatible with classical tidal theories, and reinforce the need for more complex dissipation models to describe the interior dynamics of giant planets.

Acknowledgements. A.M., L.G.C., M.Z. and P.T. aknowledge financial support from the Italian Space Agency through the Agreement 2021-13-HH.1-2023 (Europa Clipper). A.M, L.G.C, M.Z and P.T. moreover wish to acknowledge Caltech and the Jet Propulsion Labora- tory for granting the University of Bologna a license to an executable version of the MONTE project edition software.

References

Bar-Sever, Y. E., Jacobs, C. S. Keihm, S., et al. 2007, Proc. IEEE, 95, 2180
Cooper, N. J., Murray, C. D., Lainey, V., et al. 2014, A&A, 572, A8
Cooper, N. J., Lainey, V., Meunier, L.-E., et al. 2018, A&A, 610, A2
Ćuk, M., Dones, L., & Nesvorný, D. 2013, arXiv e-prints [arXiv:1311.6780]
Dermott, S. F. 1979, Icarus, 37, 310
Desmars, J., Vienne, A., & Arlot, J.-E. 2009, A&A, 493, 1183
Durante, D., Hemingway, D. J., Racioppa, P., Iess, L., & Stevenson, D. J. 2019, Icarus, 326, 123
Evans, S., et al. 2018, CEAS Space Journal, 10, 79
Folkner, W. M., Williams, J. G., Boggs, D. H., Park, R. S., & Kuchynka, P. 2014, IPN Prog. Rep., 196, 42
French, R. G., et al. 2006, PASP, 118, 246
French, R. G., McGhee-French, C. A., Lonergan, K., et al. 2017, Icarus, 290, 14
Fuller, J., Luan, J., & Quataert, E. 2016, MNRAS, 458, 3867
Goldreich, P., & Nicholson, P. D. 1977, Icarus, 30, 301
Goossens, S., van Noort, B., Mateo, A., Mazarico, E., & van der Wal, W. 2024, Nat. Astron., 8, 846
Iess, L., Jacobson, R. A., Ducci, M., et al. 2012, Science, 337, 457
Iess, L., Militzer, B., Kaspi, Y., et al. 2019, Science, 364, eaat2965
Jacobson, R. A. 2022, AJ, 164, 199
Lainey, V., Noyelles, B., Cooper, N., et al. 2019, Icarus, 326, 48
Lainey, V., Casajus, L. G., Fuller, J., et al. 2020, Nat. Astron., 4, 1053
Lainey, V., Rambaux, N., Cooper, N., Dahoumane, R., & Zhang, Q. 2023, A&A, 670, L25
Magnanini, A. 2021, Aerotecnica Missili & Spazio, 100, 195
Magnanini, A., Zannoni M., Casajus, L. G., et al. 2024, A&A, 687, A132
Magnanini, A., Zannoni, M., & Lainey, V. 2026, A&A, 707, A96
Mignard, F. 1979, Moon Planets, 20, 301
Oberti, P., Veillet, C., & Catullo, V. 1989, A&AS, 80, 289
Park, R. S., Folkner, W. M., Williams, J. G., & Boggs, D. H. 2021, AJ, 161, 105
Park, R. S., Jacobson, R. A., Gomez Casajus, L., et al. 2025, Nature, 638, 69
Petricca, F., et al. 2025, Nature, 648, 556
Robert, V., et al. 2016, A&A, 596, A37
Tajeddine, R., Cooper, N. J., Lainey, V., et al. 2013, A&A, 551, A129
Tajeddine, R., Lainey, V., Cooper, N. J., et al. 2015, A&A, 575, A73
Tanga, P., Pauwels, T., Mignard, F., et al. 2023, A&A, 674, A12
Tortora, P., Zannoni, M., Hemingway, D., et al. 2016, Icarus, 264, 264
Veiga, C. H., & Vieira Martins, R. 2000, A&AS, 143, 405
Veiga, C. H., Vieira, M. R., Vienne, A., et al. 2003, A&A, 400, 1095
Yelle, R. V., Strobell, D. F., Lellouch, E., & Gautier, D. 1997, ESA SP, 1177, 243
Zannoni, M., Hemingway, D., Casajus, L. G., & Tortora, P. 2020, Icarus, 345, 113713
Zhang, Q. F., et al. 2018, MNRAS, 481, 98

Appendix A: Radio tracking residuals

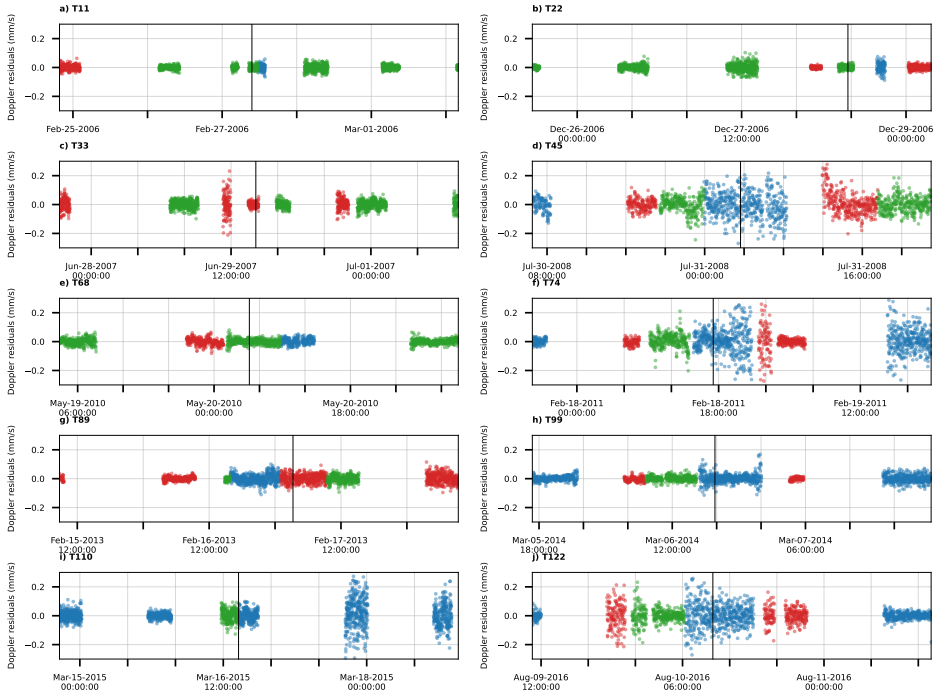

Fig. A.1: Range-rate residuals integrated over 60 s. Panels (a-j) show the corresponding range-rate data for each arc.

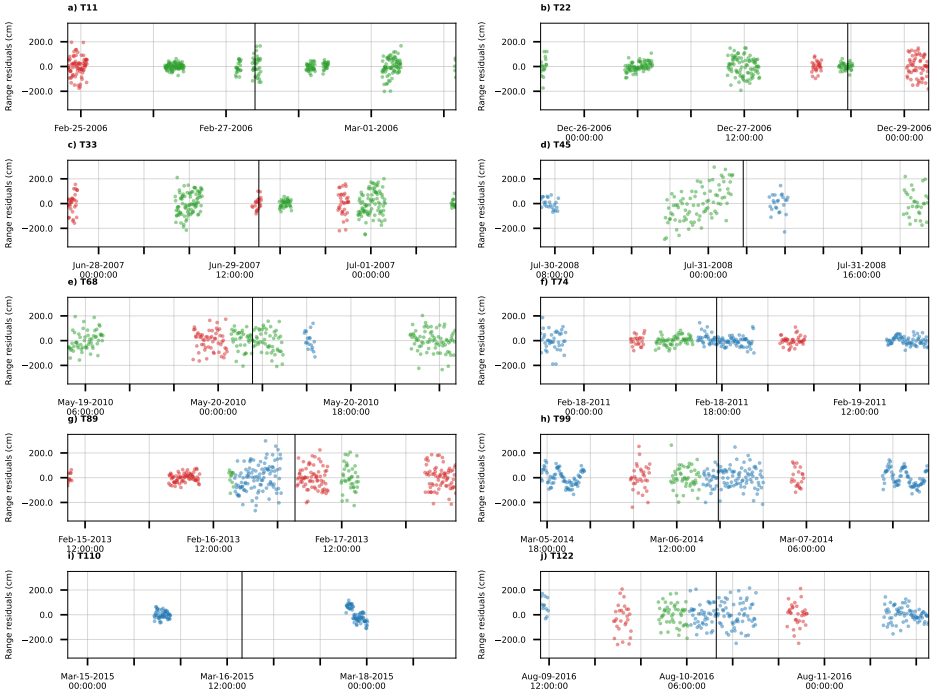

Fig. A.2: Range residuals integrated over 60 s. Panels (a-j) show the corresponding range-rate data for each arc.

Appendix B: Astrometry data and normal point residuals

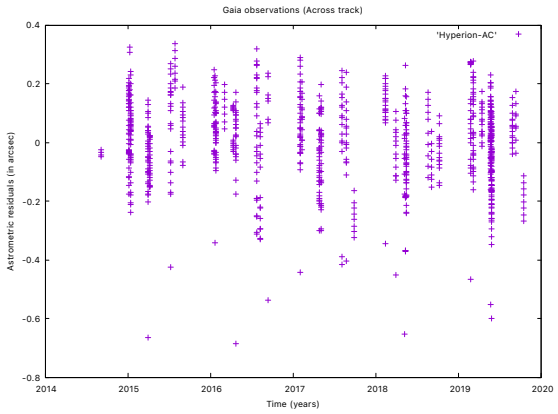

(a)

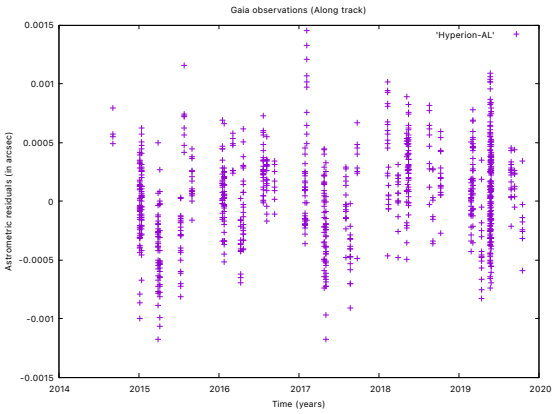

(b)

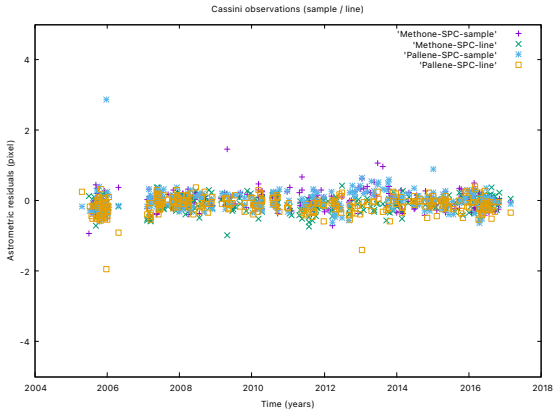

(c)

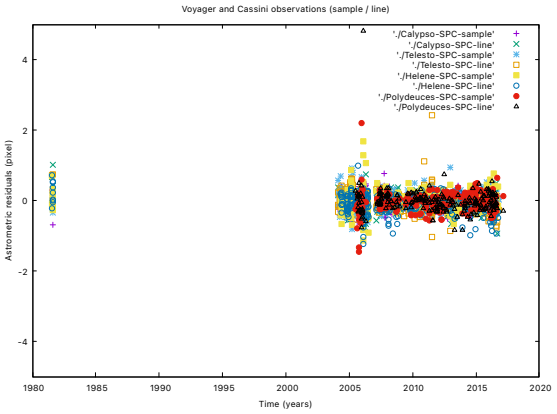

(d)

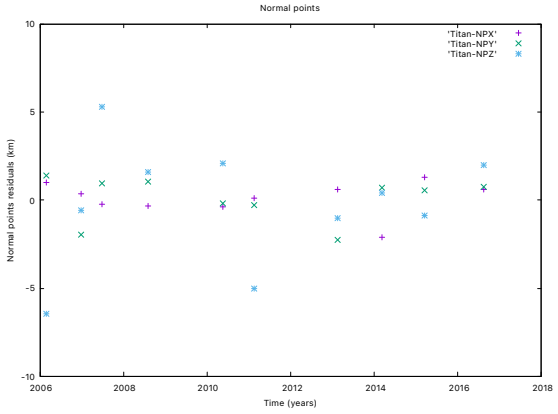

(e)

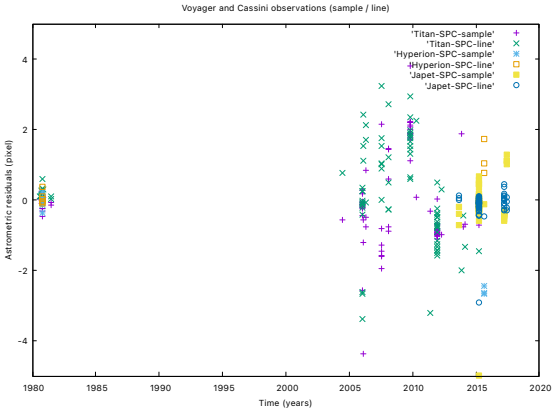

(f)

Fig. B.1: Astrometric and normal point residuals for Titan, Hyperion, Iapetus, and the small Saturnian moons used in this analysis. The panels display *Gaia* observations of Hyperion (a, b), Cassini and Voyager imaging residuals for the small and Lagrangian moons (c, d), and the outer major moons (f), along with the Cassini radio science normal points for Titan (e). The variance and covariance matrices of Titan's state at the times of the Cassini flybys can be provided upon request.

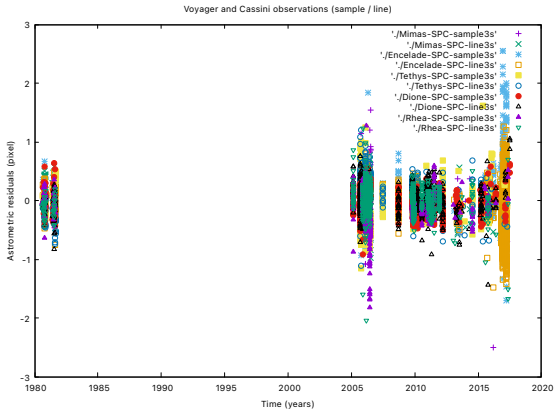

(a)

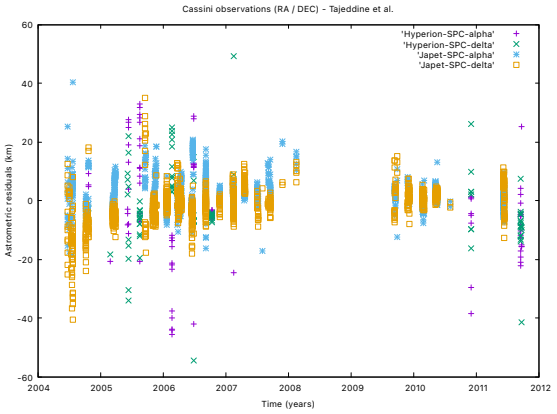

(b)

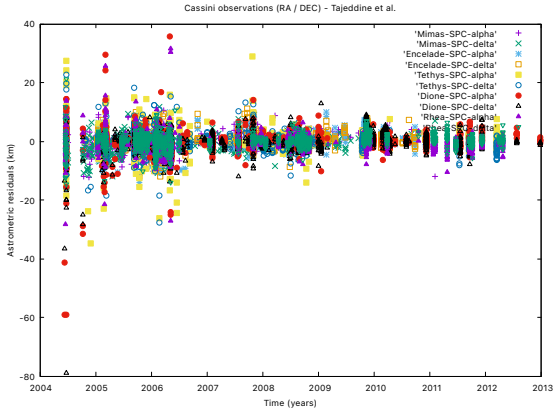

(c)

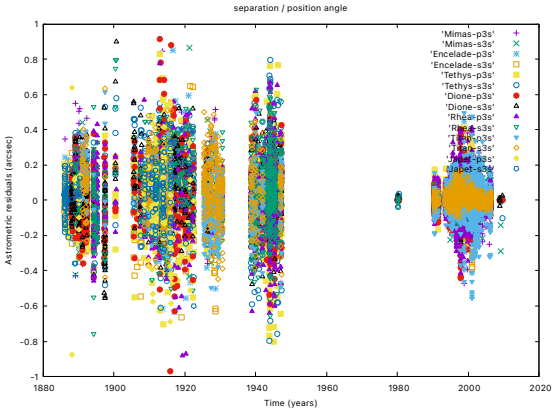

(d)

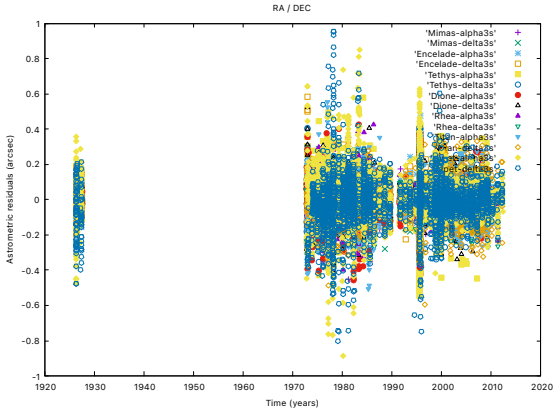

(e)

Fig. B.2: Astrometric residuals for the main inner Saturnian satellites. The panels display Cassini and historical imaging residuals in sample and line (a), right ascension and declination (b, c, e), and separation and position angle (d) primarily for Mimas, Enceladus, Tethys, Dione, and Rhea.

B.1. Global fit estimated masses

Table B.1: Comparison of estimated Saturnian system GMs.

Parameter	**Jacobson (2022)** (3σ)	**This Work** (3σ)
GM_{Saturn}	37 931 206.234 ± 0.726	37 931 207.124 ± 2.169
GM_{Mimas}	2.50349 ± 0.00042	2.503620 ± 0.000067
$GM_{\text{Enceladus}}$	7.21037 ± 0.00027	7.207680 ± 0.008242
GM_{Tethys}	41.21353 ± 0.00094	41.213338 ± 0.000323
GM_{Dione}	73.11607 ± 0.00016	73.115888 ± 0.000165
GM_{Rhea}	153.94175 ± 0.00123	154.292858 ± 0.609825
GM_{Titan}	8 978.13710 ± 0.00074	8 978.15300 ± 0.04084
GM_{Hyperion}	0.37049 ± 0.00015	0.353062 ± 0.036933
GM_{Iapetus}	120.51511 ± 0.00727	121.350366 ± 5.652801
GM_{Helene}	0.00048 ± 0.00005	0.000658 ± 0.000154

Notes. Comparison between estimated Saturnian system GMs from Jacobson (2022) and this work. All uncertainties are 3σ. Values are in km^3s^{-2}.

Appendix C: Radio science's normal points

Table C.1: Reduced cartesian normal points of Titan with respect to Saturn in the EME2000 frame.

		Position (km)			**Velocity (km/s)**		
Flyby	**Epoch (ET)**	$X \pm \sigma_X$	$Y \pm \sigma_Y$	$Z \pm \sigma_Z$	$D_X \pm \sigma_{D_X}$	$D_Y \pm \sigma_{D_Y}$	$D_Z \pm \sigma_{D_Z}$
T011	2006-02-27 08:26:24	-1094713.8 ± 1.3	614775.3 ± 2.7	55112.7 ± 3.6	-2.633834 ± 1.7 × 10^{-5}	-4.700197 ± 7.5 × 10^{-6}	0.54913 ± 3.8 × 10^{-5}
T022	2006-12-28 10:06:27	-1245135.9 ± 0.33	125269.3 ± 3.5	101430.1 ± 8.4	-0.463474 ± 2.6 × 10^{-5}	-5.386096 ± 7.2 × 10^{-6}	0.40451 ± 7.2 × 10^{-5}
T033	2007-06-29 17:00:51	1177979.7 ± 0.22	-120269.6 ± 2.5	-95827.2 ± 5.9	0.589153 ± 1.8 × 10^{-5}	5.682258 ± 1.1 × 10^{-5}	-0.43562 ± 4.4 × 10^{-5}
T045	2008-07-31 02:14:16	963735.0 ± 2.9	-693230.9 ± 3.7	-38181.9 ± 8.0	3.278509 ± 2.4 × 10^{-5}	4.660746 ± 1.6 × 10^{-5}	-0.60414 ± 1.3 × 10^{-4}
T068	2010-05-20 03:25:26	505222.1 ± 0.79	1101755.9 ± 1.1	-118958 ± 14	-4.994961 ± 1.3 × 10^{-5}	2.496426 ± 1.2 × 10^{-5}	0.27167 ± 3.1 × 10^{-5}
T074	2011-02-18 16:05:17	-974649.3 ± 0.66	789738.6 ± 1.4	32544 ± 14	-3.424316 ± 2.3 × 10^{-5}	-4.165677 ± 1.8 × 10^{-5}	0.58345 ± 8.4 × 10^{-5}
T089	2013-02-17 01:57:42	756628.8 ± 5.2	933593.6 ± 4.8	-129487.7 ± 4.2	-4.269855 ± 1.9 × 10^{-5}	3.672108 ± 2.5 × 10^{-5}	0.12892 ± 9.8 × 10^{-5}
T099	2014-03-06 16:27:54	788092.0 ± 6.5	905231.7 ± 5.6	-130261.0 ± 0.90	-4.146062 ± 2.2 × 10^{-5}	3.821132 ± 2.7 × 10^{-5}	0.10878 ± 1.0 × 10^{-4}
T110	2015-03-16 14:30:55	-830127.7 ± 8.3	-905696.3 ± 6.7	133948.1 ± 6.4	4.148352 ± 2.6 × 10^{-5}	-3.623083 ± 2.9 × 10^{-5}	-0.12285 ± 1.0 × 10^{-4}
T122	2016-08-10 08:32:01	293705.2 ± 5.4	-1165628.6 ± 1.0	52094.9 ± 8.0	5.429423 ± 9.2 × 10^{-5}	1.483605 ± 2.6 × 10^{-5}	-0.57890 ± 5.1 × 10^{-5}

Notes. The table displays the corresponding 1σ uncertainties for the provided values.

Table C.2: Comparison of Titan's estimated gravity-field parameters with respect previous analyses.

Parameter ($\times 10^{-6}$)	**This Work**	Durante et al. (2019)	Petricca et al. (2025)	Goossens et al. (2024)
J_2	33.973 ± 0.710	33.089 ± 0.609	33.511 ± 0.471	36.256 ± 3.108
C_{21}	0.183 ± 0.255	0.513 ± 0.215	0.483 ± 0.116	−0.738 ± 0.261
C_{22}	10.306 ± 0.101	10.385 ± 0.084	10.107 ± 0.062	11.263 ± 1.285
S_{21}	−0.083 ± 0.478	0.612 ± 0.359	0.695 ± 0.263	−1.082 ± 0.625
S_{22}	0.014 ± 0.081	−0.064 ± 0.066	0.053 ± 0.052	0.515 ± 0.143
J_3	0.026 ± 1.000	−0.179 ± 0.720	0.992 ± 0.612	0.628 ± 1.199
C_{31}	1.275 ± 0.317	1.481 ± 0.254	1.909 ± 0.175	1.045 ± 0.346
C_{32}	0.264 ± 0.233	0.183 ± 0.153	−0.260 ± 0.129	0.720 ± 0.322
C_{33}	−0.220 ± 0.029	−0.222 ± 0.017	−0.233 ± 0.018	−0.113 ± 0.031
S_{31}	−0.488 ± 0.551	0.811 ± 0.402	1.318 ± 0.323	−3.363 ± 0.705
S_{32}	0.083 ± 0.142	−0.027 ± 0.099	0.391 ± 0.060	−0.337 ± 0.216
S_{33}	−0.222 ± 0.026	−0.226 ± 0.019	−0.231 ± 0.019	−0.099 ± 0.030
J_4	0.982 ± 1.945	−1.077 ± 1.844	2.056 ± 1.425	−3.074 ± 2.640
C_{41}	−0.367 ± 0.318	−0.842 ± 0.299	−0.473 ± 0.149	−0.285 ± 0.492
C_{42}	0.242 ± 0.133	0.183 ± 0.107	−0.007 ± 0.077	1.132 ± 0.202
C_{43}	−0.048 ± 0.050	−0.012 ± 0.039	−0.131 ± 0.025	0.031 ± 0.059
C_{44}	−0.009 ± 0.004	0.014 ± 0.003	−0.011 ± 0.003	−0.003 ± 0.005
S_{41}	−1.275 ± 0.850	0.191 ± 0.717	−0.527 ± 0.546	−3.868 ± 1.053
S_{42}	0.205 ± 0.134	0.198 ± 0.106	0.513 ± 0.067	−0.206 ± 0.157
S_{43}	−0.014 ± 0.037	−0.062 ± 0.033	−0.086 ± 0.030	−0.046 ± 0.051
S_{44}	−0.009 ± 0.004	−0.012 ± 0.004	−0.004 ± 0.003	0.002 ± 0.005
J_5	1.019 ± 2.198	1.118 ± 2.022	3.008 ± 1.467	−4.762 ± 3.270
C_{51}	0.144 ± 0.405	0.361 ± 0.406	0.240 ± 0.268	0.340 ± 0.535
C_{52}	0.031 ± 0.134	−0.097 ± 0.118	−0.056 ± 0.064	0.347 ± 0.184
C_{53}	−0.012 ± 0.023	−0.016 ± 0.019	−0.057 ± 0.012	0.061 ± 0.030
C_{54}	−0.003 ± 0.005	0.007 ± 0.004	0.004 ± 0.003	0.003 ± 0.006
C_{55}	0.001 ± 0.000	0.000 ± 0.001	0.000 ± 0.001	−0.001 ± 0.001
S_{51}	−0.667 ± 0.722	0.267 ± 0.604	−0.028 ± 0.481	−1.587 ± 0.830
S_{52}	0.156 ± 0.115	0.044 ± 0.094	0.173 ± 0.069	−0.159 ± 0.156
S_{53}	−0.007 ± 0.016	−0.004 ± 0.012	0.003 ± 0.011	0.067 ± 0.019
S_{54}	−0.003 ± 0.005	−0.002 ± 0.004	−0.005 ± 0.004	−0.019 ± 0.007
S_{55}	0.001 ± 0.001	0.000 ± 0.001	0.001 ± 0.001	0.000 ± 0.001
Parameter (unscaled)				
k_2	0.596 ± 0.094	0.616 ± 0.067	0.608 ± 0.048	0.375 ± 0.060

Notes. Parameters are unnormalized, with a reference radius of 2575 km, derived from the radio science local analysis used to generate the normal points. All reported uncertainties are 1σ.

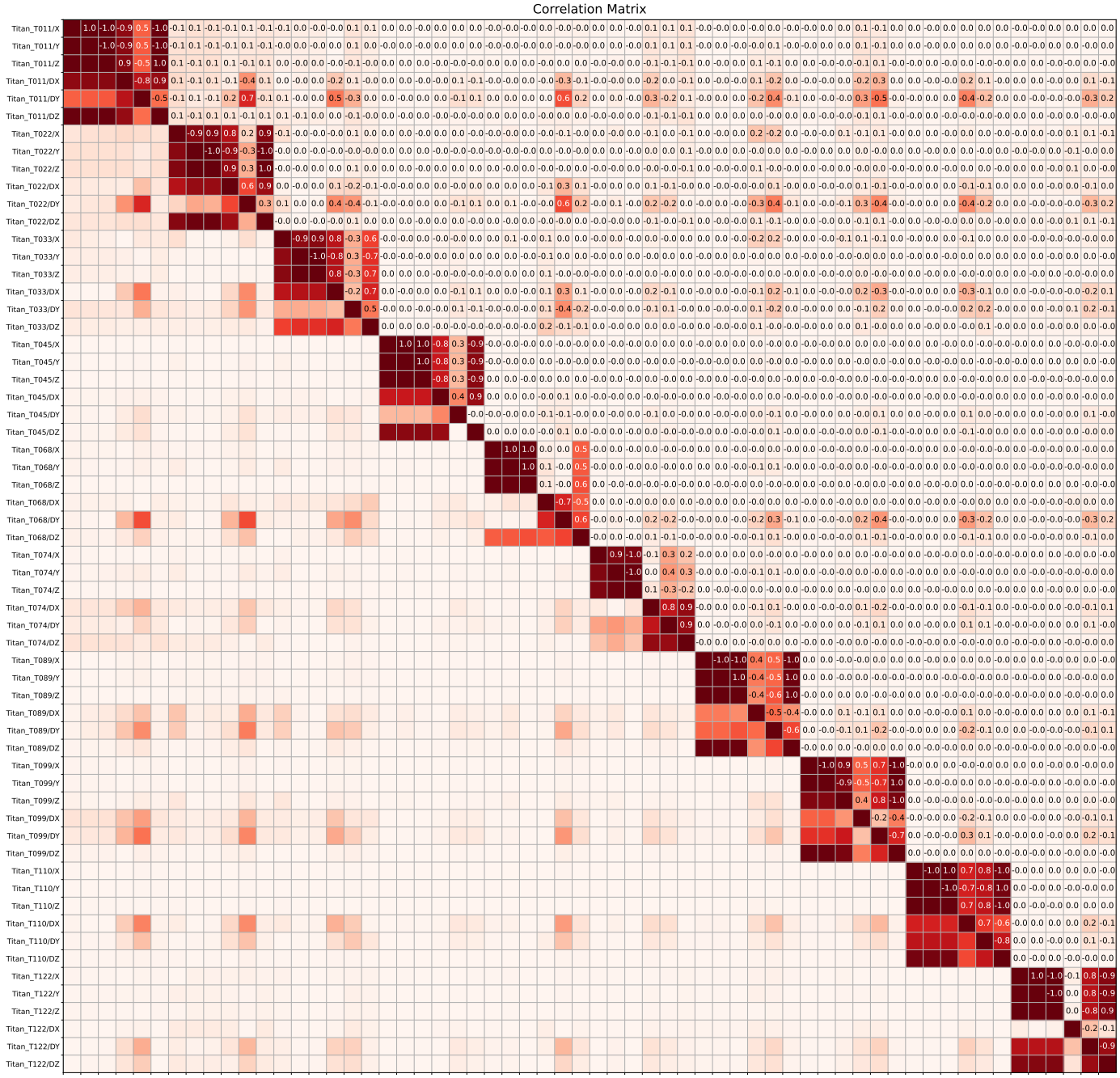

Fig. C.1: Radio science normal point correlation matrix.